Irregular Grid Finite-Difference Techniques: Simulations of Oscillations in Shallow Circular Basins

W. C. THACKER

Atlantic Oceanographic and Meteorological Laboratories, NOAA, Sea-Air Interaction Laboratory, Miami, Fla. 33149

(Manuscript received 13 February 1976, in revised form 23 September 1976)

ABSTRACT

Finite-difference techniques for irregular computational grids are presented. Successful simulations of transient normal mode oscillations in shallow circular basins, where analytic solutions are known, demonstrate that these techniques can yield accurate results, even in situations involving a curved boundary. These techniques should prove to be quite useful for numerically forecasting storm surges in bays and estuaries where calculations are complicated by the curving coastline.

1. Introduction

Numerical forecasts of storm surges in bays, estuaries or lakes are complicated by the curvature of the coastline. Straightforward finite-difference calculations (Reid and Bodine, 1968; Overland, 1975) on uniform, rectangular computational grids, which represent the coastline as a stair-step boundary, may yield well-behaved solutions away from the boundary but generate numerical noise at the coastline where the forecast is to be made. Coordinate transformation techniques (Reid and Vastano, 1966; Birchfield and Murty 1974; Jelesnianski, 1974) provided a better representation of the boundary. However, the effort involved in defining the transformation makes it difficult to implement. Finite-element methods (Wang and Conner, 1975; Norton, King, and Orlob, 1973) with irregular, triangular computational grids also provide a better representation of the boundary. However, they are time-implicit and require lengthy matrix inversion at each time step which is undesirable for forecast models. This suggests that time-explicit, finite-difference calculations on irregular, triangular grids might be a way to handle the problem of boundary curvature.

To date, little has been done to implement finite-difference techniques on irregular triangular grids. Kivisild (1954) used a grid of equilateral triangles to calculate storm surges on Lake Okeechobee. Crowley (1971), Boris *et al.* (1975) and Fritts (1976) have made finite-difference calculations using irregular grids. They were concerned with problems other than storm surge forecasting where there is an advantage that the grid points be free to move during the calculation. There seems to be no discussion in the literature of these techniques per se. For this reason, emphasis here is placed on the techniques rather than on storm surges. However, the discussion will be restricted to two-dimensional grids and to the shallow water wave equations so that the applicability to storm surge forecasting can be seen.

The approximation of partial derivatives on irregular grids is discussed in Section 2. The basic idea is that the partial derivatives can be approximated by the slopes of a planar surface. This idea can be generalized so that an average of slopes of several planar surfaces can be used to approximate derivatives. Such approximations are first order in the grid spacings. Although higher order schemes are possible based upon the slopes of parabolic or other surfaces, they are not discussed in detail. The formulas for approximating partial derivatives have the desirable feature of satisfying a Green's theorem. For shallow water waves this guarantees that mass is conserved.

Two different schemes for approximating solutions to the shallow water wave equations are discussed. The first scheme involves two spatially staggered grids, one for the water surface elevation and the other for the momentum. This scheme yields good results when the earth's rotation is neglected, but it cannot be used when these terms must be included. The second scheme has only one grid for all variables and allows rotation to be included.

Numerical solutions to the shallow water wave equations for a circular basin calculated with these schemes are compared to corresponding exact solutions obtained analytically in closed form. Computations are initialized to normal modes of the basin and carried forward for a time approximately equal to 50 cycles of the normal mode. After 50 cycles, both the amplitudes and the frequencies of the computations are in good agreement with the exact values for the normal modes. This demonstrates that these irregular grid finite-difference

techniques do indeed provide a means for incorporating curved boundaries into numerical calculations and suggests that these techniques might be useful for forecasting storm surges.

2. Formulas for approximating partial derivatives

An irregular two-dimensional grid can be thought of as being a patchwork of triangular elements whose vertices are the grid points. In the vicinity of each triangle, the partial derivatives of a function can be approximated by the slopes of a plane determined by the values of the function at the vertices. This leads to the following three-point formulas for approximating partial derivatives:

$$\left.\begin{aligned}\overline{\frac{\partial f}{\partial x}}&=[f_1(y_2-y_3)+f_2(y_3-y_1)+f_3(y_1-y_2)]/\Delta\\ \overline{\frac{\partial f}{\partial y}}&=-[f_1(x_2-x_3)+f_2(x_3-x_1)+f_3(x_1-x_2)]/\Delta\\ \Delta&=x_1(y_2-y_3)+x_2(y_3-y_1)+x_3(y_1-y_2)\end{aligned}\right\}, \quad (1)$$

where f_1, f_2 and f_3 are the values of the function at the three vertex points, (x_1,y_1), (x_2,y_2) and (x_3,y_3), respectively. The overbars indicate that these are approximations. The quantity Δ is twice the area of the triangle.

The accuracy of these formulas depends upon the point (x,y) at which the derivatives are approximated, even though the formulas do not explicitly depend upon that point. Clearly the approximation is better in the vicinity of the triangle than at some distance point. The dependence of the accuracy upon the point (x,y) can be seen by considering power series expansions of the function about that point, i.e.,

$$\left.\begin{aligned}f_1&=f+\frac{\partial f}{\partial x}(x_1-x)+\frac{\partial f}{\partial y}(y_1-y)+\epsilon_1\\ f_2&=f+\frac{\partial f}{\partial x}(x_2-x)+\frac{\partial f}{\partial y}(y_2-y)+\epsilon_2\\ f_3&=f+\frac{\partial f}{\partial x}(x_3-x)+\frac{\partial f}{\partial y}(y_3-y)+\epsilon_3\end{aligned}\right\}, \quad (2)$$

where ϵ_1, ϵ_2, and ϵ_3 are higher order terms of the expansions. Solving for $\partial f/\partial x$ and $\partial f/\partial y$ yields corrections to (1),

$$\left.\begin{aligned}\frac{\partial f}{\partial x}&=\overline{\frac{\partial f}{\partial x}}-[\epsilon_1(y_2-y_3)+\epsilon_2(y_3-y_1)+\epsilon_3(y_1-y_2)]/\Delta\\ \frac{\partial f}{\partial y}&=\overline{\frac{\partial f}{\partial y}}+[\epsilon_1(x_2-x_3)+\epsilon_2(x_3-x_1)+\epsilon_3(x_1-x_2)]/\Delta\end{aligned}\right\}. \quad (3)$$

The terms ϵ_j are of second order in the grid spacing and the correction terms in (3) are therefore of first order. Even if the point (x,y) is at the center of an equilateral triangle, the correction terms are first order in the grid spacing, in contrast to the case of centered differences on uniform rectangular grids in which the correction terms are second order. However, the approximation is best at the centers of the triangles, $x=(x_1+x_2+x_3)/3$ and $y=(y_1+y_2+y_3)/3$.

The approximation to the derivatives expressed by (1) is equivalent to the approximations involved in using linear interpolating functions for finite element calculations. Higher order polynomial interpolating functions have a counterpart of higher order finite-difference approximations. The partial derivatives can be approximated by the slopes of polynomial surfaces determined by some greater number of grid points. For example, if the midpoint of each side of the triangles is also a grid point, the values of the function at each vertex and each side point of a triangle determine a parabolic surface. In this case the slope approximation does depend explicitly upon the point (x,y) where the approximation is made. In this case, the same procedure of power series expansions will yield six-point functions and their corrections, as in (3). However, no effort has been made to proceed along these lines.

These three-point formulas are best suited for approximating derivatives at the centers of the triangular elements comprising the grid. When staggered grids can be used, as in Section 3, where the centers of the triangles of one grid are the vertices of the other, then there is no difficulty other than an ambiguity due to the fact that, generally, there are more centers than vertices. It is desirable in this case to approximate the derivatives at the vertices rather than at the centers.

Each grid point is simultaneously the vertex of several triangles. The derivatives at that grid point might be approximated by the three-point formulas for any of these triangles. This suggests that an average of these formulas should be used. Because the triangles are not all the same size, the average should be weighted by the areas of the triangles. If these are N triangles with a vertex at (x,y) and their remaining vertices at (x_1,y_1), ..., (x_N,y_N) are indexed counterclockwise about (x,y), then this averaging procedure yields the N point formulas

$$\left.\begin{aligned}\overline{\frac{\partial f}{\partial x}}&=\sum_{i=1}^{N} f_i(y_{i+1}-y_{i-1})/\Delta\\ \overline{\frac{\partial f}{\partial y}}&=-\sum_{i=1}^{N} f_i(x_{i+1}-x_{i-1})/\Delta\\ \Delta&=\sum_{i=1}^{N} x_i(y_{i+1}-y_{i-1})\end{aligned}\right\}, \quad (4)$$

where the summation is cyclic, modulo N, and Δ is twice the area of the polygon formed by the N triangles.

For the case $N=3$, the N point formulas reduce to the three-point formulas of Eqs. (1). For the case in which the polygon $N=4$, is a rectangle, Eqs. (4) reduce to the usual centered-difference formulas. These formulas do not depend explicitly upon the point (x,y) where the derivatives are approximated; again, the accuracy does depend upon that point. The accuracy, still first order, is best at the centroid of the polygon formed by the N triangles.

Formulas (4) can be rewritten

$$\left.\begin{aligned}\overline{\frac{\partial f}{\partial x}}&=\sum_{i=1}^{N}\tfrac{1}{2}(f_i+f_{i+1})(y_{i+1}-y_i)/\tfrac{1}{2}\Delta\\ \overline{\frac{\partial f}{\partial y}}&=-\sum_{i=1}^{N}\tfrac{1}{2}(f_i+f_{i+1})(x_{i+1}-x_i)/\tfrac{1}{2}\Delta\end{aligned}\right\},\qquad(5)$$

so that each term can be associated with a triangle side connecting points i and $i+1$. The first factor, $\frac{1}{2}(f_i+f_{i+1})$, is the average value of the function for the side. Note that this side is shared by two triangles, unless it lies on a boundary. Therefore, because the points are taken counter-clockwise in the formulas, the terms associated with this line are equal in magnitude but opposite in sign at the two triangles where these terms contribute. This fact guarantees that a Green's theorem is satisfied.

Green's theorem (see, e.g., Taylor, 1955) states that, for two functions f and g with continuous first partial derivatives in a region R bounded by a sectionally smooth curve c,

$$\int\int\left(\frac{\partial f}{\partial x}+\frac{\partial g}{\partial y}\right)dxdy=\int_c(fdy-gdx).\qquad(6)$$

On an irregular triangular grid, the corresponding theorem is

$$\tfrac{1}{3}\sum_{i=1}^{M}\left(\overline{\frac{\partial f}{\partial x}}+\overline{\frac{\partial g}{\partial y}}\right)_i\tfrac{1}{2}\Delta_i=\sum_{i=1}^{B}\left[\tfrac{1}{2}(f_i+f_{i+1})(y_{i+1}-y_i)-\tfrac{1}{2}(g_i+g_{i+1})(x_{i+1}-x_i)\right].\qquad(7)$$

Here it is assumed that there are M grid points and that the first B points are on the boundary and indexed counterclockwise. The factor $\frac{1}{2}\Delta_i$ is the area of the polygon formed by the triangles with a vertex at the point i. Because each triangle has three vertices, only one-third of this area can be associated with each vertex; thus the factor $\frac{1}{3}$. Using the fact from the preceding paragraph, it is easy to see that when evaluating the left-hand side of (7) using (5), the contributions of the internal lines cancel, leaving only the contribution of the boundary on the right-hand side of (7).

A similar Green's theorem holds for the three-point formulas of (1) on staggered grids. When applied to shallow water waves, these theorems guarantee that the total volume of water is constant so long as no water flows in at the boundary.

So far, only approximations for first partial derivatives have been discussed. One possibility for approximating higher derivatives is by iterating the formulas for the first derivatives. However, this approximation might depend upon the order of the differentiation, in which case $\overline{\partial^2 f/\partial x\partial y}\neq\overline{\partial^2 f/\partial y\partial x}$. This is the case for the three-point formulas on staggered grids, even if the grids are composed of identical triangular elements. On regular grids, four- and six-point formulas can be iterated to form second derivatives, but for irregular grids $\overline{\partial^2 f/\partial x\partial y}\neq\overline{\partial^2 f/\partial y\partial x}$. Therefore, iterating the formulas for first derivatives does not seem attractive.

If the first derivatives had been approximated by the slopes of higher order polynomials, then the curvature of these polynomials would provide an approximation to the second derivatives. This corresponds to the fact that higher order interpolating functions must be used with the finite-element method to approximate solutions to partial differential equations involving higher derivatives.

These results for two-dimensional irregular grids can be generalized to higher dimensions. For k dimensions, the basic approximation yields $(k+1)$ point formulas. Again, averaging should provide approximations for derivatives at the grid points. Higher order approximations to first derivatives might also be constructed, as well as higher partial derivatives.

3. Two irregular grid schemes for shallow water waves

The linearized shallow water wave equations in the absence of frictional stresses are

$$\left.\begin{aligned}\frac{\partial U}{\partial t}&=-gD\frac{\partial H}{\partial x}+fV\\ \frac{\partial V}{\partial t}&=-gD\frac{\partial H}{\partial y}-fU\\ \frac{\partial H}{\partial t}&=-\left(\frac{\partial U}{\partial x}+\frac{\partial V}{\partial y}\right)\end{aligned}\right\},\qquad(8)$$

where U and V are the x and y components of volume transport per unit width, H is the surface elevation, D the stillwater depth, g the gravitational acceleration and f the Coriolis parameter accounting for the earth's rotation. Two irregular grid, finite-difference schemes were used to calculate approximate solutions to these equations for the case of a closed circular basin. The first involved the use of staggered grids, one for U and V and the other for H. In the second scheme all three variables were calculated at the same grid points.

Samples of grids used for these calculations are shown in Figs. 1, 2 and 3. For scheme one, the vertices of the

triangles were taken as grid points for U and V, and the crosses at the centers of alternate triangles as those for H. (The crosses have been omitted from Fig. 3 because of the small scale of the elements.) For scheme two, U, V and H are all calculated at the vertex points. For both schemes, there are U, V points situated on the boundary so that the zero normal flow condition is easy to implement.

It is interesting to note that these grids are topologically equivalent to hexagonal arrays of equilateral triangles. An interior hexagonal pattern is quite evident in the interior of grid 1, but the outer triangles have been distorted to approximate the circular basin. The hexagonal pattern which can easily be recognized near the center of grids 2 and 3 is gradually distorted to the circular shape at the boundary. Because of this topological equivalence, these calculations are equivalent to coordinate transformation calculations on a hexagonal shaped grid of equilateral triangles.

The manner in which the grid points are indexed is unimportant. The convention followed was to index the U, V points with a single integer, $i=1, \ldots, I$, with the boundary points first, $i=1, \ldots, B$, and the H points with the integer, $j=1, \ldots, J$. What is important is to know which points are neighbors so that the finite-difference formulas can be evaluated. For scheme one, arrays were used to store the indices of the three H points closest to each U, V point and the indices of the three U, V points closest to each H point. For scheme two, six neighbor indices were stored for interior points and four or five for boundary points, depending upon the number of triangles which meet at that point.

The finite-difference formulas depend upon the coordinates of the grid points. For numerical stability (see Section 4) it is important that the grid points be smoothly distributed. The smooth distributions for

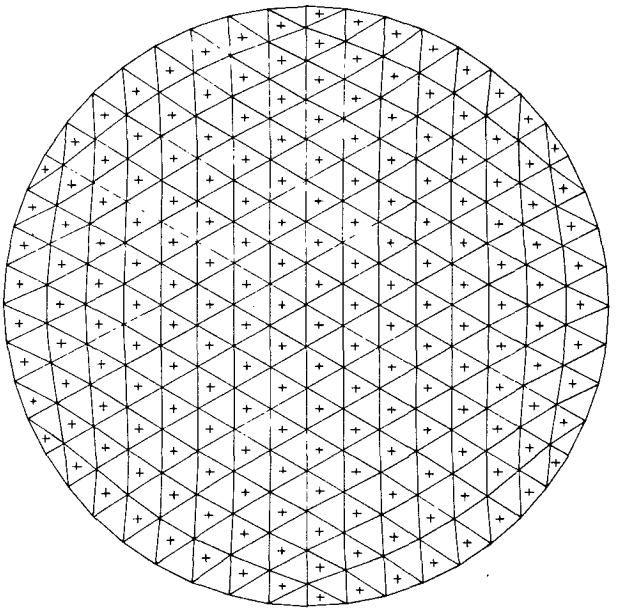

FIG. 2. Grid two. U, V and H are calculated as for grid one. Instabilities associated with nonuniformity of the triangles were insignificant.

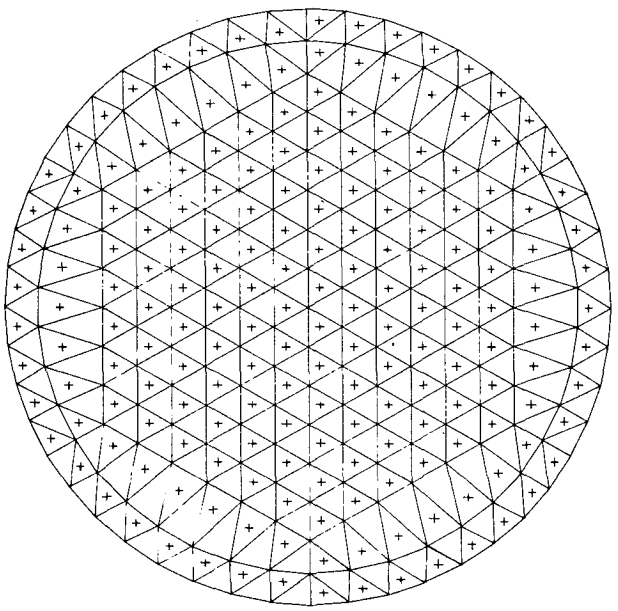

FIG. 1. Grid one. The transports U and V are calculated at the vertices of the triangles. For scheme one, the surface elevation H is calculated at the centers of the triangles marked by crosses; for scheme two, at the vertices the same as U and V. The contrast in triangle sizes is greater for this grid than for grid two, resulting in a larger growth rate for the associated instability.

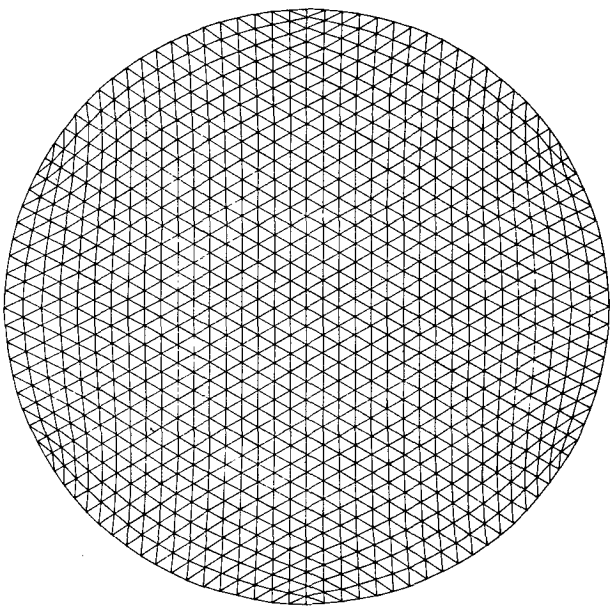

FIG. 3. Grid three. U, V and H are calculated as for grid one, the crosses marking scheme one H points being omitted because of scale. This grid provided quite good resolution of the normal modes which were simulated.

grids 2 and 3 were obtained by solving the equations

$$\left.\begin{aligned} x_i &= \tfrac{1}{6}\sum_{n=1}^{6} x_{i_n(i)} \\ y_i &= \tfrac{1}{6}\sum_{n=1}^{6} y_{i_n(i)} \end{aligned}\right\}, \quad i=B+1, \ldots, I, \tag{9}$$

where $i_n(i)$, $n=1, \ldots, 6$, are the six neighboring points to the ith point on the U, V grid. Some of the neighboring points can be boundary points with coordinates, $x_i=R\cos(2\pi i/B)$ and $y_i=R\sin(2\pi i/B)$, $i=1, \ldots, B$. Eqs. (9) can be thought of as determining the equilibrium position of a system of springs under tension, fixed at the boundary points. These equations were solved using an over-relaxed Jacobi technique. The staggered H-grid coordinates were then given by

$$\left.\begin{aligned} x_j &= \tfrac{1}{3}\sum_{n=1}^{3} x_{i_n(j)} \\ y_j &= \tfrac{1}{3}\sum_{n=1}^{3} y_{i_n(j)} \end{aligned}\right\}, \quad j=1, \ldots, J, \tag{10}$$

where $i_n(j)$, $n=1, \ldots, 3$, are the three points on the U, V-grid closest to the jth point on the staggered H-grid.

For both schemes, the discrete analogues of (8) take the form

$$\left.\begin{aligned}
U_i^{n+\frac{1}{2}} &= U_i^{n-\frac{1}{2}} - gD_i\tau\left(\overline{\frac{\partial H}{\partial x}}\right)_i^n + f\tau V_i^{n+\frac{1}{2}} \\
V_i^{n+\frac{1}{2}} &= V_i^{n-\frac{1}{2}} - gD_i\tau\left(\overline{\frac{\partial H}{\partial y}}\right)_i^n - f\tau U_i^{n+\frac{1}{2}}
\end{aligned}\right\}, \quad i=B+1, \ldots, I$$

$$\left.\begin{aligned}
U_i^{n+\frac{1}{2}} &= U_i^{n-\frac{1}{2}} - gD_i\tau\left[\sin^2\theta_i\left(\overline{\frac{\partial H}{\partial x}}\right)_i^n - \cos\theta_i\sin\theta_i\left(\overline{\frac{\partial H}{\partial y}}\right)_i^n\right] \\
V_i^{n+\frac{1}{2}} &= V_i^{n-\frac{1}{2}} - gD_i\tau\left[\cos^2\theta_i\left(\overline{\frac{\partial H}{\partial y}}\right)_i^n - \cos\theta_i\sin\theta_i\left(\overline{\frac{\partial H}{\partial x}}\right)_i^n\right]
\end{aligned}\right\}, \quad i=1, \ldots, B$$

$$H_j^{n+1} = H_j^n - \tau\left[\left(\overline{\frac{\partial U}{\partial x}}\right)_j^{n+\frac{1}{2}} + \left(\overline{\frac{\partial V}{\partial g}}\right)_j^{n+\frac{1}{2}}\right], \quad j=1, \ldots, J \tag{11}$$

In scheme one, the three-point formulas were used to approximate the partial derivatives; $(\overline{\partial H/\partial x})_i^n$ and $(\overline{\partial H/\partial y})_i^n$ were calculated using the three H points nearest to the U point, i, and $(\overline{\partial U/\partial x})_j^{n+\frac{1}{2}}$ and $(\overline{\partial V/\partial y})_j^{n+\frac{1}{2}}$ were calculated using the three U, V-points nearest to the H point, j. For the boundary points, $i=1, \ldots, B$, the three closest H points form triangles which do not intersect the boundary; the slopes of these triangles were extrapolated to the boundary. In scheme two, with $i\equiv j$ and $I\equiv J$, six-point formulas were used to approximate the partial derivatives except for points on the boundary, $i=j=1, \ldots, B$. Five-point formulas were used for all boundary points except for six corresponding to the corners of distorted hexagons for which four-point formulas were used.

The trigonometric factors $\cos\theta_i$ and $\sin\theta_i$ guarantee that there is no normal flow at the boundary. A leap-frog scheme was used for the time derivatives, with surface elevations calculated at times $t=n\tau$ and momentum components calculated at times $t=(n+\frac{1}{2})\tau$, where τ is the length of the time step and $n=0, 1, 2, \ldots$. The time differences are implicit since the Coriolis terms are evaluated at the new time levels, $n+\frac{1}{2}$, in order to guarantee stability in the limit, $g=0$. No time-consuming matrix inversion is necessary, though, since the equations are only coupled by pairs; it is a simple matter to rewrite the equations expressing $U_i^{n+\frac{1}{2}}$ and $V_i^{n+\frac{1}{2}}$ in terms of H_i^n, and $U_i^{n-\frac{1}{2}}$ and $V_i^{n-\frac{1}{2}}$.

4. Numerical stability

By assuming the grids to be uniform and without boundaries, it is possible to analyze these two computational schemes for stability. For equilateral triangular grids, the solutions can be assumed to vary as $\exp\{i[(2M+N)k\Delta+\sqrt{3}Nl\Delta]\}$, where 2Δ is the distance between grid points, k and l are wave vector components, and the integers M and N index the grid points. For both schemes the eigenvalues λ of the amplification matrices must satisfy equations of the form

$$\left.\begin{aligned}
&(1-\lambda)[(1+f^2)\lambda^2-(2-p)\lambda+1]-iq\lambda^2=0 \\
&p=4gD(\tau^2/\Delta^2)(|z_1|^2+|z_2|^2) \\
&q=(8/\sqrt{3})fgD(\tau^2/\Delta^2)\,\mathrm{Im}z_1^*z_2
\end{aligned}\right\}, \tag{12}$$

where $i=\sqrt{-1}$ and the complex numbers z_1 and z_2 account for the geometry of the grid,

$$\left.\begin{aligned} z_1&=1-\exp(-2ik\Delta)\\ z_2&=\tfrac{1}{2}[1+\exp(-2ik\Delta)]-\exp[i(k+\sqrt{3}l)\Delta]\end{aligned}\right\},\ \text{Scheme one}$$
$$\left.\begin{aligned} z_1&=(1/2\sqrt{3})\cos(k\Delta)\sin(l\Delta)\\ z_2&=\tfrac{1}{6}\sin(k\Delta)[2\cos(k\Delta)+\cos(\sqrt{3}l\Delta)]\end{aligned}\right\},\ \text{Scheme two}\qquad (13)$$

For scheme one, if $f=0$, then $|\lambda|\leqslant 1$ for $\tau\leqslant(\Delta/3)(gD)^{\frac{1}{2}}$. Thus, when the earth's rotation is neglected, scheme one is stable so long as the time step is small enough. This corresponds to the usual Courant condition for rectangular grids. For $f\neq 0$, because $q\neq 0$, scheme one is unstable. To see this, note that for small f, the eigenvalue corresponding to $\lambda=1$ when $f=0$ becomes $\lambda=1-iq/p$, so $|\lambda|^2=1+q^2/p^2>1$. Thus, scheme one is unstable when the earth's rotation is included. The fact that $q\neq 0$ seems to be related to the fact that $\overline{\partial^2 H/\partial x\partial y}\neq\overline{\partial^2 H/\partial y\partial x}$, even on a uniform grid, where these second derivatives are approximated by iterating the approximations for first derivatives. As the solutions step forward in time, these terms do not cancel, so they provide a numerical source of vorticity and energy. For the case $f=0$ these terms never appear.

For scheme two, $q=0$. The Courant condition follows from the inequality $2[1-(1+f^2)^{\frac{1}{2}}]\leqslant p\leqslant 2[1+(1+f^2)^{\frac{1}{2}}]$. Thus, the Coriolis force increases the upper bound on the time step but it imposes a lower bound. So long as this Courant condition is satisfied, scheme two is stable—even when the earth's rotation is included.

The fact that these schemes are stable for uniform grids does not guarantee their stability for variable grids with boundaries. In fact, when calculations were first made on the grid shown in Fig. 1 using scheme one, instability was observed. When these calculations were repeated on the grid shown in Fig. 2, the instability was considerably suppressed.

Instabilities associated with variable grid spacing are quite like those associated with variable coefficients on uniform grids. In fact, because the grids used here can be deformed into hexagonal arrays of equilateral triangles, the calculations could be made using a coordinate transformation technique on these uniform triangular grids. In that case, the variability of the original grid would be replaced by the variability of the map factors of the transformation to the uniform grid. The instability could be attributed to the variability of the map factor coefficients.

Instabilities associated with grid irregularities should not be identified with the fact that these are finite-difference techniques. Similar effects have been reported for finite-element calculations by Wang and Conner (1975) and by Pagenkopf and Pearce (1975). In fact, the grid smoothing technique given by Eqs. (9) which were used to position the points on grids 2 and 3 might be equally as useful for smoothing grids for finite element calculations.

Calculations with scheme two exhibited instabilities with growth rates depending upon the magnitude of f. This can be attributed to the variability of the grid spacing. For irregular grids, terms proportional to $f[(\overline{\partial^2 H/\partial x\partial y})-(\overline{\partial^2 H/\partial y\partial x})]$ provide a numerical source of energy. Thus, increasing f should increase the growth rate. For most practical problems, the growth rate is quite small. In high latitudes where f is largest, this scheme might not be feasible for highly irregular grids. Perhaps higher order schemes suitable for approximating higher partial derivatives would be more suitable in these situations.

For practical problems such as storm surge forecasting, instability should not be a problem. So long as the size of the triangles on the grid vary smoothly enough, the e-folding time due to instabilities should be on the order of a week while the duration of the surge is usually less than 24 h. The same relaxation procedure used to position the grid points in Figs. 2 and 3 can also be used to obtain smoothly varying grids for practical problems. Furthermore, when bottom friction is included in the calculations, the instability can be expected to be damped.

5. Normal mode simulations

The irregular grid finite-difference schemes described in Section 3 were used to simulate the normal mode oscillations of a closed circular basin of uniform depth $D=D_0$. These oscillations are solutions to the shallow water equations of the form (Lamb, 1945)

$$\left.\begin{aligned} H&=\eta J_n(kr)\cos(n\theta+\omega t)\\ U&=\eta\left(\frac{\omega}{k}\right)\left\{\left[\frac{n}{kr}J_n(kr)+\frac{f}{\omega}J_n'(kr)\right]\sin\theta\cos(n\theta+\omega t)-\left[\frac{n}{kr}\frac{f}{\omega}J_n(kr)+J_n'(kr)\right]\cos\theta\sin(n\theta+\omega t)\right\}\\ V&=-\eta\left(\frac{\omega}{k}\right)\left\{\left[\frac{n}{kr}J_n(kr)+\frac{f}{\omega}J_n'(kr)\right]\cos\theta\cos(n\theta+\omega t)+\left[\frac{n}{kr}\frac{f}{\omega}J_n(kr)+J_n'(kr)\right]\sin\theta\sin(n\theta+\omega t)\right\}\end{aligned}\right\},\qquad (14)$$

TABLE 1. Scheme one simulations, $f=0$, uniform depth circular basin.

Normal mode n	Normal mode m	Nondimensional frequency $=\omega R(gD_0)^{-\frac{1}{2}}$ Exact	Grid 2	Grid 3
0	1	3.8317	3.8	3.83
0	2	7.0156	6.9	7.02
0	3	10.1735	~10	10.1
0	4	13.3237	~13	13.2
1	0	1.8412	1.8	1.84
1	1	5.3314	5.3	5.33
1	2	8.5363	~ 8.3	8.54
1	3	11.7060	~12	11.6
2	0	3.0542	3.0	3.06
2	1	6.7061	~ 6.7	6.71
2	2	9.9695	~10	9.9
2	3	13.1703	~13	13.0

where η is the amplitude of the oscillation, J_n and J_n' are the Bessel function of order n and its derivative, and $x=r\cos\theta$, $y=r\sin\theta$. The values of the eigenfrequency ω and corresponding wavenumber k are determined by the dispersion equation and the boundary condition

$$\left.\begin{aligned}&\omega^2=gD_0k^2+f^2\\&kRJ_n'(kR)+\frac{nf}{\omega}J_n(kR)=0\end{aligned}\right\}. \tag{55}$$

The lowest frequency normal modes are fairly well resolved by the grids shown in Figs. 1 and 2, and therefore might be expected to be fairly well approximated for several periods of oscillation by these finite-difference schemes.

For each normal mode, the calculations were initialized according to (14) with $\eta=1$ and $t=0$ and then stepped forward in time according to (11) for 50 cycles of the normal mode oscillation. The time steps for the simulations were $\tau=0.65l(gD_0)^{-\frac{1}{2}}$, where l is the distance between adjacent points on the boundary.

During the 50 cycles of each normal mode simulation, tallies were kept of the number of times each H_j changed sign in order to judge how well the eigenfunctions were approximated. Because of discretization error, the estimates of frequency were expected to vary from grid point to grid point with the variation especially noticeable near the nodes of the eigenfunctions.

TABLE 2. Scheme two simulations, $f=0$, uniform depth circular basin.

Normal mode n	Normal mode m	Nondimensional frequency $=\omega R(gD_0)^{-\frac{1}{2}}$ Exact	Grid 3
0	1	3.8317	3.79
0	2	7.0156	6.88
0	3	10.1735	9.77
0	4	13.3237	12.3

TABLE 3. Scheme two simulations, $f=0.3(gD_0)^{\frac{1}{2}}/R$, uniform depth circular basin.

Normal mode n	Normal mode m	Nondimensional frequency $=\omega R(gD_0)^{-\frac{1}{2}}$ Exact	Grid 3
0	1	3.8434	3.81
0	2	7.0220	6.89
0	3	10.1779	9.78
0	4	13.3271	12.4
1	0	1.9748	1.94
1	1	5.3507	5.30
1	2	8.5458	8.30
1	3	11.7121	11.1

This was indeed the case, and the frequency estimate variation was considerably less for calculations on the finer grid which has less discretization error.

Results of simulations with scheme one are summarized in Table 1. Because scheme one is unstable when $f\neq 0$, only the case of $f=0$ is considered. The integers n and m identify the normal modes which were simulated; n refers to the order of the Bessel function for that mode, corresponding to the number of radial nodes, and m indicates the number of concentric circular nodes. The exact nondimensional frequencies were taken from tabulated values of zeros of derivatives of Bessel functions given by Abramowitz and Segun (1970). The tilde is used to indicate qualitatively good results having quite a bit of scatter in values of frequency estimates over the grid points. The additional resolution of grid 3 over grid 2 reduces the scatter in frequency estimates and confines it to nodal areas of higher frequency modes.

Results of simulations with scheme two are shown in Tables 2, 3 and 4 for $f=0$, $f=0.3(gD_0)^{\frac{1}{2}}/R$ and $f=1.0(gD_0)^{\frac{1}{2}}/R$, respectively. The frequency estimates are systematically low. This should be expected since the averages over neighboring triangles involved in the definition of the N point formulas (4) behave numerically like viscosity. The magnitude of the computational viscosity was estimated to be $\nu\approx 0.3(4R^2gD)^{\frac{1}{2}}$. The exact frequencies in Table 2 are the same as those in Table 1; those in Tables 3 and 4 were obtained by numerically solving (15).

During these simulations, the normal modes were approximated in amplitude and shape as well as in

TABLE 4. Scheme two simulations, $f=1.0(gD_0)^{\frac{1}{2}}/R$, uniform depth circular basin.

Normal mode n	Normal mode m	Nondimensional frequency $=\omega R(gD_0)^{-\frac{1}{2}}$ Exact	Grid 3
0	1	3.9600	3.83
0	2	7.0865	6.88
0	3	10.2225	9.78
0	4	13.3612	12.30

frequency. During the phase of the oscillation when the surface should be flat, variation in the surface due to discretization error was apparent, but this variation was small compared to the maximum amplitude of the surface elevation. As expected, these schemes conserve the quantity of water in the basin. However, because of the weak instabilities associated with irregularities of the grids, after more than 50 cycles the amplitudes and shapes, like the frequencies, are poorly simulated.

In order to test the behavior of these irregular grid finite-difference schemes for situations when the depth of the basin is not uniform, normal modes of a circular basin with a parabolic depth profile $D=D_0[1-(r^2/R)]$ were also simulated. These oscillations are of the form (see Lamb, 1945),

$$\left.\begin{aligned} H&=\eta\left(\frac{r}{R}\right)^n\Psi_{m,n}\left(\frac{r}{R}\right)\cos(n\theta+\omega t)\\ U&=-\eta\frac{gD}{(\omega-f)R}\left(\frac{r}{R}\right)^{n-1}\left\{n\Psi_{m,n}\left(\frac{r}{R}\right)\sin[(n-1)\theta+\omega t]+\frac{r}{R}\Psi'_{m,n}\left(\frac{r}{R}\right)\left[\left(\frac{\omega}{\omega+f}\right)\cos\theta\sin(n\theta+\omega t)\right.\right.\\ &\qquad\left.\left.-\left(\frac{f}{\omega+f}\right)\sin\theta\cos(n\theta+\omega t)\right]\right\}\\ V&=-\eta\frac{gD}{(\omega-f)R}\left(\frac{r}{R}\right)^{n-1}\left\{n\Psi_{m,n}\left(\frac{r}{R}\right)\cos[(n-1)\theta+\omega t]+\frac{r}{R}\Psi'_{m,n}\left(\frac{r}{R}\right)\left[\left(\frac{\omega}{\omega+f}\right)\sin\theta\sin(n\theta+\omega t)\right.\right.\\ &\qquad\left.\left.+\left(\frac{f}{\omega+f}\right)\cos\theta\cos(n\theta+\omega t)\right]\right\}\end{aligned}\right\},\quad(16)$$

where $\Psi_{m,n}(r/R)=F(-m, m+n+1; n+1; r^2/R^2)$ is a hypergeometric polynomial and $\Psi'_{m,n}(r/R)$ is its derivative with respect to r/R. The integers m and n indicate the number of concentric circular nodes and the number of diametrical nodes, respectively, of the H fieid. The freqencies of these oscillations are given by solutions of the dispersion equation

$$(\omega^2-f^2)\frac{R}{gD_0}+2n\left(\frac{\omega-f}{\omega}\right)=4(m+1)(m+n).\quad(17)$$

Four oscillations were simulated using both schemes with grid three. The initial conditions were determined by Eqs. (16) and (17) with $\eta=1$ and $t=0$. For the modes with $m=0$, $\Psi_{0,n}=1$ and $\Psi'_{0,n}=0$ for all values of r/R. For the modes with $n=0$,

$$\Psi_{m,0}(r/R)=P_n(1-2r^2/R^2)$$

is a Legendre polynomial; in particular

$$\Psi_{1,0}(r/R)=1-2r^2/R^2$$

(see Lamb, 1945, or Abramowitż and Stegun, 1970). As before, the time step was taken to be $\tau=0.65l(gD_0)^{-\frac{1}{2}}$.

The results of simulations using scheme one $[f=0]$ are given in Table 5. Those for scheme two $[f=0$ and $f=0.3(gD_0)^{\frac{1}{2}}/R]$ are given in Tables 6 and 7, respectively. These results are as good as those for the uniform depth basin. Neither scheme has difficulty with depth variations.

6. Discussion

The simulations of normal mode oscillations provide particularly appropriate tests of the irregular grid finite-difference techniques since these techniques are intended for future use in modeling storm surges. The shallow water wave equations which govern these oscillations are the basis of storm surge calculations. There are other terms which must be added to these equations to account for atmospheric forcing of the water motion, dissipation due to bottom stress, and perhaps nonlinearities if the amplitude of the motion is sufficiently

TABLE 5. Scheme one simulations, $f=0$, parabolic depth circular basin.

Normal mode		Nondimensional frequency $=\omega R(gD_0)^{-\frac{1}{2}}$	
n	m	Exact	Grid 3
1	0	1.4142	1.41
2	0	2.0000	2.00
3	0	2.4495	2.43
0	1	2.8284	2.83

TABLE 6. Scheme two simulations, $f=0$, parabolic depth circular basin.

Normal mode		Nondimensional frequency $=\omega R(gD_0)^{-\frac{1}{2}}$	
n	m	Exact	Grid 3
1	0	1.4142	1.41
2	0	2.0000	1.99
3	0	2.4495	2.43
0	1	2.8284	2.80

TABLE 7. Scheme two simulations, $f=0.3(gD_0)^{\frac{1}{2}}/R$, parabolic depth circular basin.

Normal mode		Nondimensional frequency $=\omega R(gD_0)^{-\frac{1}{2}}$	
n	m	Exact	Grid 3
1	0	1.5721	1.57
2	0	2.1556	2.14
3	0	2.6041	2.58
0	1	2.8443	2.83

great, but since the exact solutions to the equations with these terms added are not available for comparison, discussion of simulations of these effects will be postponed until further calculations are made which are appropriate to a particular bay. The success of the normal mode simulations indicates that these irregular grid techniques do provide a means for calculating when there are curved boundaries such as the curving coastlines of bays and estuaries and that there are no difficulties associated with variations of the depth of the basin or with rotation of the earth. Furthermore, these simulations show that the transient response to initial conditions can be accurately represented, which is important for storm surge simulation.

Although the primary motivation for these irregular grid techniques has been the problem of curved boundaries, another advantage of these techniques is that they allow for a variation in the density of grid points over the domain of the calculation. This is desirable for storm surge models for two reasons. Because the explicit time step is bounded by the smallest ratio of grid spacing to square root of depth, on a uniform grid it is controlled by the greatest depths situated farthest from the coastline where the forecast is to be made. Variable grid spacing should allow for a larger time step to be used that is equally appropriate for shallow as for deep regions of the basin. Second, because wavelengths contract as waves propagate into shallower water, the variable grid spacing would also allow for the same number of grid points per wavelength in all parts of the basin. Plans exist for investigating the use of such a grid in conjunction with calculations for a particular bay.

Finally, it should be emphasized that these irregular grid finite-difference techniques are quite general and should be useful for a wide variety of calculations. They offer the same flexibility as do the irregular grid finite-element techniques, and they have the advantage of an explicit time step which is useful for computations of transient phenomena.

REFERENCES

Abramowitz, Milton, and Irene A. Stegun, Eds., 1970: *Handbook of Mathematical Functions*. Nat. Bur. Stnds., 411 pp.

Birchfield, G. E., and T. S. Murty, 1974: A numerical model for wind-driven circulation in Lakes Michigan and Huron. *Mon. Wea. Rev.*, **102**, 157–165.

Boris, J. P., K. L. Hain and M. J. Fritts, 1975: Free surface hydrodynamics using a Lagrangian triangular mesh. *Proc. First Intern. Conf. Numerical Ship Hydrodynamics*, 20–23 October, David W. Taylor Naval Ship Research and Development Center.

Crowley, W. P., 1971: FLAG: A free-Lagrange method for numerically similating hydrodynamic flows in two dimensions. *Proc. Second Inter. Conf. Numerical Methods in Fluid Dynamics*. Springer-Verlag.

Fritts, Martin, (1976). A numerical study of free surface waves. Rep. SAI-76-528-WA, Science Applications, Inc. (To be submitted to *Phys. Fluids*.)

Jelesnianski, Chester P., (1974). SPLASH (Special program to list amplitudes of surges from hurricanes) Part two. General track and variant storm conditions. NOAA Tech. Memo. NWS TDL-52.

Kivisild, Hans R., 1954: Wind effect on shallow bodies of water with special reference to Lake Okeechobee. *Trans. Roy. Inst. Tech. Sweden*, **83**.

Lamb, Horace, 1945: *Hydrodynamics*. Dover Publ., Sections 191, 193, 210, 212.

Norton, William R., Ian P. King and Gerald T. Orlob, 1973. A finite element model for lower granite reservoir. Final report prepared for Walla Walla District, U. S. Army Corps of Engineers, Walla Walla, Wash.

Overland, James E., 1975: Estimation of hurricane storm surge in Apalachicola Bay, Florida. NOAA Tech. Rep. NWS 17.

Pagenkopf, James R., and Bryan P. Pearce, 1975: Evaluation of techniques for numerical calculation of storm surges. Tech. Rep. No. 199, Ralph M. Parsons Laboratory for Water Resources and Hydrodynamics, MIT.

Reid, Robert O., and Bernie R. Bodine, 1968: Numerical model for storm surges in Galveston Bay. *J. Waterways Harbors Div. Proc. ASCE*, **94**, 33–57.

Reid, R. O., and A. C. Vastano, 1966: Orthogonal coordinates for the analysis of long gravity waves near islands. *Coastal engineering, Proc. Santa Barbara Specialty Conf.*, Amer. Soc. Civil Eng., 1–20.

Taylor, Angus E., (1955). *Advanced Calculus*. Ginn and Company, Chap. 13.

Wang, John D., and Jerome J. Conner, 1975: Mathematical modeling of near coastal circulation. MIT Sea Grant Program Rep. No. MITSG 75-13.